Monthly Notices
of the
ROYAL ASTRONOMICAL SOCIETY

MNRAS **451,** 4238–4252 (2015) doi:10.1093/mnras/stv1130

The VLT Survey Telescope ATLAS

T. Shanks,[1]★ N. Metcalfe,[1] B. Chehade,[1] J. R. Findlay,[1] M. J. Irwin,[2] E. Gonzalez-Solares,[2] J. R. Lewis,[2] A. Kupcu Yoldas,[2] R. G. Mann,[3] M. A. Read,[3] E. T. W. Sutorius[3] and S. Voutsinas[3]

[1]*Physics Department, University of Durham, South Road, Durham DH1 3LE, UK*
[2]*Institute of Astronomy, University of Cambridge, Madingley Road, Cambridge B3 0HA, UK*
[3]*Institute for Astronomy, University of Edinburgh, Blackford Hill, Edinburgh EH9 3HJ, UK*

Accepted 2015 May 15. Received 2015 May 15; in original form 2015 February 18

ABSTRACT

The VLT Survey Telescope ATLAS survey is an optical *ugriz* survey aiming to cover ≈4700 deg^2 of the southern sky to similar depths as the Sloan Digital Sky Survey (SDSS). From reduced images and object catalogues provided by the Cambridge Astronomical Surveys Unit, we first find that the median seeing ranges from 0.8 arcsec FWHM (full width at half-maximum) in *i* to 1.0 arcsec in *u*, significantly better than the 1.2–1.5 arcsec seeing for SDSS. The 5σ mag limit for stellar sources is $r_{AB} = 22.7$ and in all bands these limits are at least as faint as SDSS. SDSS and ATLAS are more equivalent for galaxy photometry except in the *z* band where ATLAS has significantly higher throughput. We have improved the original ESO magnitude zero-points by comparing $m < 16$ star magnitudes with the AAVSO Photometric All-Sky Survey in *gri*, also extrapolating into *u* and *z*, resulting in zero-points accurate to $\approx \pm 0.02$ mag. We finally compare star and galaxy number counts in a 250 deg^2 area with SDSS and other count data and find good agreement. ATLAS data products can be retrieved from the ESO Science Archive, while support for survey science analyses is provided by the OmegaCAM Science Archive, operated by the Wide-Field Astronomy Unit in Edinburgh.

Key words: catalogues – surveys – cosmology: observations – large-scale structure of Universe.

1 INTRODUCTION

The ATLAS survey (Shanks et al. 2013) is carried out on the VLT Survey Telescope (VST), a 2.61-m telescope situated at Cerro Paranal Observatory (Schipani et al. 2012). It uses the OmegaCAM camera (Kuijken et al 2011) containing 32 4k×2k CCDs with a total of 268 megapixels. The field of view of the camera is 1 × 1 deg^2 and the pixel size is 0.21 arcsec. The aim of the survey is to produce a *ugriz* catalogue to the equivalent depth of Sloan Digital Sky Survey (SDSS) but in the Southern hemisphere, with a target area of ≈4700 deg^2. Although the survey was only specified to have seeing in the range 1–1.4 arcsec FWHM (full width at half-maximum), with the better seeing going to the VST KiDS survey (de Jong et al. 2013), ATLAS is proving to have better median seeing than expected, at the subarcsecond level. The survey is being made alongside its sister VISTA Hemisphere Survey (VHS; McMahon et al. 2013) which is supplying the *YJK* bands. The survey depths are also well matched to the *WISE* survey (Wright et al. 2010) at the mid-IR *L* and *M* bands. The footprint of the survey is shown in Fig. 1 where it is compared to the footprints of KiDS and VHS. The deeper VISTA VIKING NIR survey (Edge et al. 2013) has approximately the same footprint as KiDS. ATLAS has yearly data releases with DR1 occurring in 2013 April and covering ≈1500 deg^2 of data taken before 2012 September 30 and DR2 now imminent and covering ≈2500 deg^2 taken before 2013 September 30.

1.1 ATLAS science aims

The primary aims of the ATLAS survey are cosmological. The UV sensitivity of the survey gives it an advantage in terms of quasar surveys that in the Southern hemisphere can be followed up using instruments like AAT 2dF or VISTA 4MOST. These surveys can then be used, for example, to look for any evidence of excess power in the quasar clustering data that might provide evidence for primordial non-Gaussianity in the early Universe. It may also be possible to search for Baryon Acoustic Oscillations at the 100 Mpc scale in the unexplored $0.8 < z < 2.2$ redshift range. These analyses can be done either by photo-*z* using selection codes like XDQSO-z (Bovy et al. 2012) or by using spectroscopic redshifts. We have already used AAT 2dF to make a redshift survey of ≈10 000 quasars using UVX and NIR selection and these are being used to study the

★ E-mail: tom.shanks@durham.ac.uk

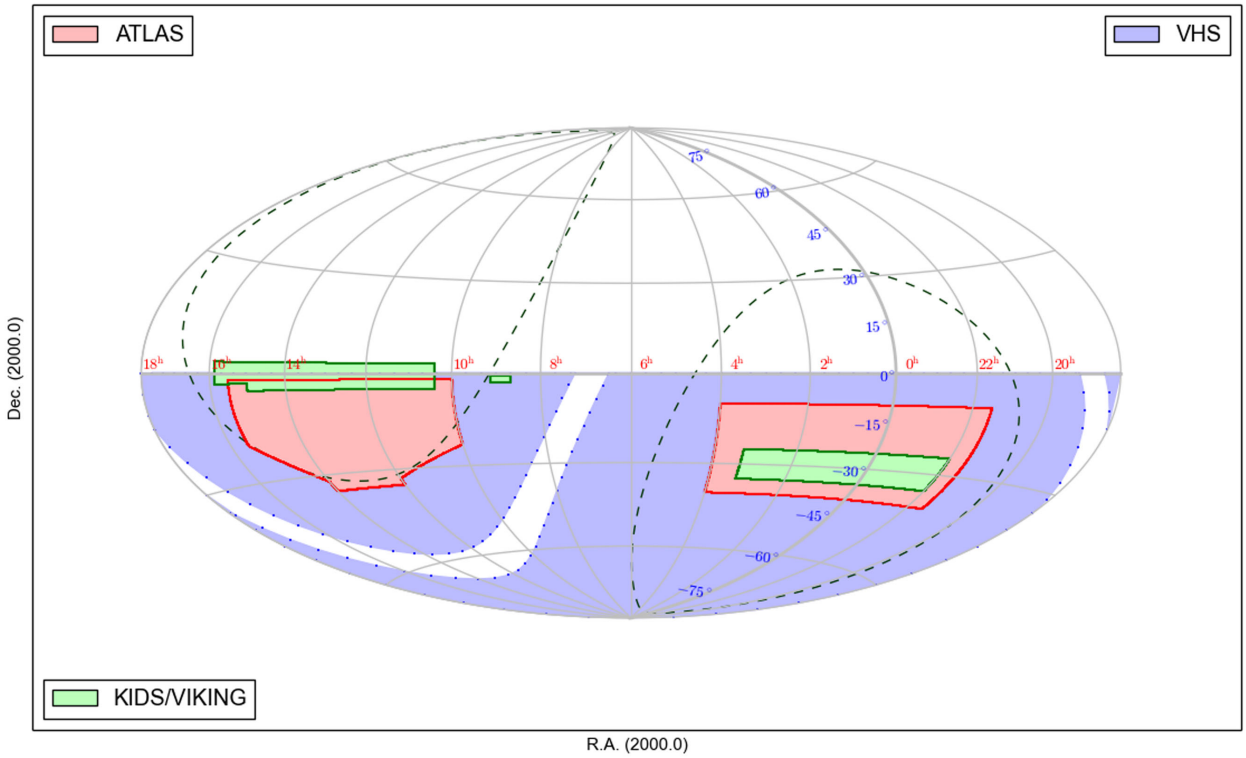

Figure 1. ATLAS footprint in equatorial coordinates (red) compared to VHS (blue/grey) and KIDS (green). VHS surveys the whole hemisphere except at ±5 deg from the Galactic plane. The dashed lines indicate $b = \pm 30$ deg.

luminosity and clustering correlation function of dusty and unobscured quasars (Chehade et al., in preparation). This quasar redshift survey can also form the base for photo-z clustering analyses over the whole VST ATLAS area. Such quasar surveys will also complement future programmes such as the X-ray AGN surveys of e-ROSITA (Merloni et al. 2012).

Another cosmological aim is to test for the Integrated Sachs-Wolfe effect by cross-correlating the 2D positions of luminous red galaxies with microwave background temperature fluctuations (e.g. Sawangwit et al. 2010). This is one of the few independent tests of the accelerating expansion of the Universe and the Southern hemisphere is the only place left to improve the statistical significance of this test.

The galaxy and quasar surveys can also be combined to study the quasar lensing magnification bias at high redshift and the quasar galaxy clustering environment at low redshifts (e.g. Mountrichas & Shanks 2007). ATLAS will also take advantage of its excellent seeing to allow many galaxy lensing shear projects. Although not as deep as KiDS, ATLAS shares the same VST platform which means that the advantages of low optical distortion are shared by ATLAS for lensing projects.

We shall also be looking at galaxy counts and how they vary over the sky at bright magnitudes. Previous observations from 2MASS have suggested that there exists a galaxy underdensity in the Southern hemisphere (Keenan, Barger & Cowie 2013; Whitbourn & Shanks 2014), and we wish to test for the existence of this 'Local Hole' at optical wavelengths. Since VST ATLAS will also cover the Great Attractor region, this means that it can use the form of bright galaxy counts to search a large area in this direction for clusters and superclusters even behind Shapley 8.

Mapping the Southern hemisphere using galaxy clusters is also another cosmological aim of VST ATLAS. The *riz* bands will be combined with VHS and *WISE* NIR bands to select galaxy clusters to $z \approx 1$.

There are many other non-cosmological projects that can be done with ATLAS. The discovery of dwarf satellite galaxies and stellar streams in the Southern hemisphere is one clear example (Belokurov et al. 2014; Koposov et al. 2014) and ATLAS is also being used to search for high-redshift quasars via the Lyman-break technique (Carnall et al. 2015).

Except where stated, we use AB magnitudes throughout the paper.

2 ATLAS DESCRIPTION

2.1 Survey area

As can be seen from Fig. 1, the ATLAS sky coverage consists of two contiguous blocks in the North and South galactic caps. The ATLAS South Galactic Cap (SGC) area lies between $21^h30^m < \mathrm{RA} < 04^h00^m$ and $-40^\circ < \mathrm{Dec} < -10^\circ$, whilst the North Galactic Cap (NGC) area lies between $10^h00^m < \mathrm{RA} < 15^h30^m$ and $-20^\circ < \mathrm{Dec} < -2.5^\circ$ plus $10^h00^m < \mathrm{RA} < 15^h00^m$ and $-30^\circ < \mathrm{Dec} < -20^\circ$. There is complete coverage of the VST KiDS survey (de Jong et al. 2013) in the SGC, but only partial coverage in the NGC. The NGC area below Dec < -20 is approved as an ESO public survey in *iz* and is approved as a Chilean ESO proposal (e.g. 095.A-0561) in *ugr*. The total area of the survey is 4711 deg^2 with 2087 deg^2 in the NGC and 2624 deg^2 in the SGC. There is also an ongoing 'Chilean u extension project' to double the exposure time in u from 2 to 4 min over the full ATLAS area (PI: L. Infante). Status maps of the ATLAS survey can be found at http://astro.dur.ac.uk/Cosmology/vstatlas/.

Table 1. ATLAS basic characteristics. ATLAS median seeing for ESO A, B classified tiles. SDSS median seeing is taken from Bramich & Freudling (2012). Mag. limit (ATLAS) corresponds to the median 5σ mag detection limit for stars as measured in a 1-arcsec radius aperture. Mag. limit (gal) corresponds to ATLAS 5σ limit now calculated in apertures of the SDSS seeing radius at airmass 1.0. SDSS mag. limit corresponds to 5σ SDSS point source detection limits based on the above fluxes and calculated in a radius of the above median SDSS seeing at airmass 1.0. Sky brightness is measured in mag arcsec^{-2}. SDSS DR1 sky brightness is median of 77 068 frames from http://www.sdss2.org/dr7/products/general/seeing.html. Fluxes are given at 20 mag for ATLAS and SDSS normalized to airmass 1.3. SDSS fluxes come from Stoughton et al. (2002, equation 1). All VST magnitudes are quoted in the SDSS AB system (allowing for the transformations in Section 3.2).

Band	*u*	*g*	*r*	*i*	*z*
ATLAS exposure (s)	2 × 60	2 × 50	2 × 45	2 × 45	2 × 45
ATLAS seeing (arcsec)	1.02	0.95	0.90	0.81	0.84
SDSS seeing (arcsec)	1.46	1.36	1.24	1.18	1.20
ATLAS mag. limit	21.99	23.14	22.67	21.99	20.87
ATLAS mag. limit (gal)	21.78	22.71	22.17	21.40	20.23
SDSS mag. limit	21.87	22.75	22.31	21.71	20.17
ATLAS sky brightness	22.34	21.90	20.92	19.78	18.85
SDSS sky brightness	22.15	21.85	20.86	20.20	19.00
ATLAS 20 mag e$^-$s^{-1}	29	177	160	101	29
SDSS 20 mag e$^-$s^{-1}	33	175	174	116	19

2.2 Survey observations

OmegaCAM camera pixels are 0.213 × 0.213 arcsec^2 in size so approximately half the dimensions of 0.396 × 0.396 arcsec^2 SDSS pixels. The *ugriz* band transmissions are shown in Fig. 2 where they are compared to those for SDSS. They are seen to be similar in all bands except for *z* where ATLAS has an ≈2 × higher throughput. The ATLAS exposure times have been conservatively increased over the typical SDSS 54 s exposure to maintain the S/N achieved by SDSS taking into account increased read-out noise and, potentially, sky brightness, particularly in *i* and *z* (see Table 1). The OmegaCAM read-out noise is typically five to six electrons per pixel and the gain is ≈2.2 with 10 per cent chip-to-chip rms. Double exposures

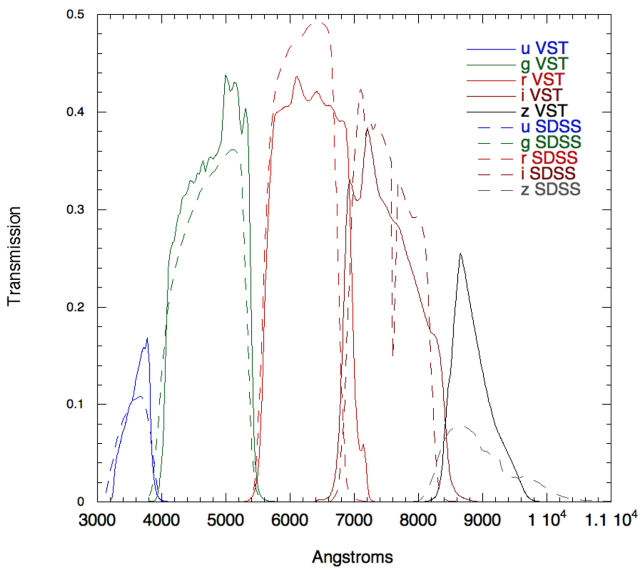

Figure 2. Filter + telescope + atmospheric transmissions for ATLAS (solid lines) and SDSS (dashed lines) for *ugriz* passbands as labelled. All are calculated at airmass 1.3. No atmospheric dispersion corrector is assumed for the ATLAS filters since it is not being used.

are taken, dithered by 85 arcsec in declination and 25 arcsec in RA, to cover the main inter-chip gaps (80.5 arcsec and 11.8 arcsec in declination and 21.5 arcsec in RA) and to allow cosmic rays to be rejected. The two-pointing dither and 2 arcmin tile overlaps leaves 28 (80.5 × 21.5 arcsec) and 14 (11.8 × 21.5 arcsec) small holes (see green areas in Fig. 4) amounting to ≈1/3 per cent of the total area. Each OmegaCAM field is ≈1 × 1 deg^2 and each tile has a 58 arcmin centre-to-centre spacing, giving an ≈2 arcmin overlap between tiles in both the RA and Dec directions.

For each VST ATLAS tile, two dithered exposures in each of the *ugr* bands were observed in dark time and two dithered exposures in each of the *iz* bands in grey/bright time. For all except the first two months of the survey, the observations were done in concatenations of 17 fields in the RA direction, which approximately filled a 1h ESO Observing Block (OB) in *u* (including overheads) and slightly less in the other bands. There were no firm constraints on scheduling the different filters on the same field at similar times, although *ugr* on a particular field are always scheduled in the same six monthly ESO observing period, as are *iz* (but not necessarily the same period as for *ugr*). Fig. 3 summarizes the distribution of timing offsets between different bands on the same field. The median time between dark time (*u*, *g* or *r*) observations on the same field is about one month, as it is for bright time (*i* and *z*). However, a sizeable fraction are observed in the same week. Between *u*, *g* or *r* and one of *i* or *z* the median is slightly longer, about six weeks. The peak around 9–10 months represents occasions when the next image has been rolled over to the following year. The seeing is specified to be <1.4 arcsec FWHM and sky transparency to be 'Clear' (<10 per cent cloud cover and transparency variations <10 per cent).

The imaging data have been reduced by the Cambridge Astronomical Survey Unit (CASU) using the VST data flow software. The images were trimmed and debiased using nightly calibration frames and then flat-fielded using accumulated monthly stacked twilight sky flats. The frames are then corrected for crosstalk and defringed if necessary. The subexposures are then automatically registered and stacked. The resulting imaging data comprise the combination of the two individual images for each of the original CCDs. Each file is in a multi-extension fits (MEF) format with an

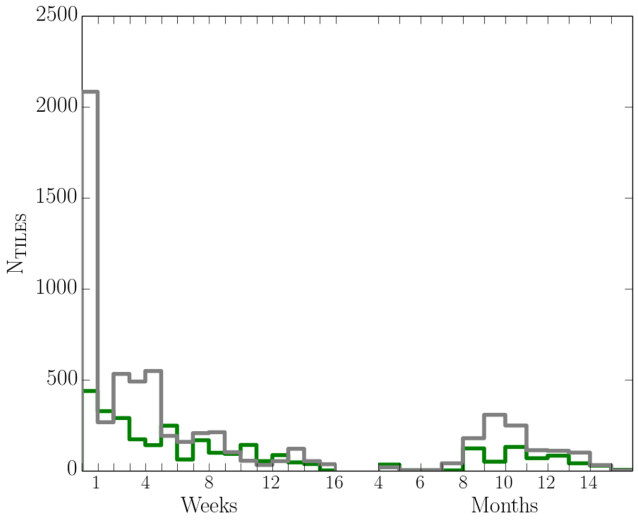

Figure 3. Grey histogram: the time delay between the first exposure on a field and the next exposure on the same field with a different filter, providing both are taken in dark time (*ugr*) or both in bright time (*iz*). Green histogram: the delay between one of *ugr* and one of *iz*, which is slightly longer as *ugr* and *iz* are always taken at different moon phase.

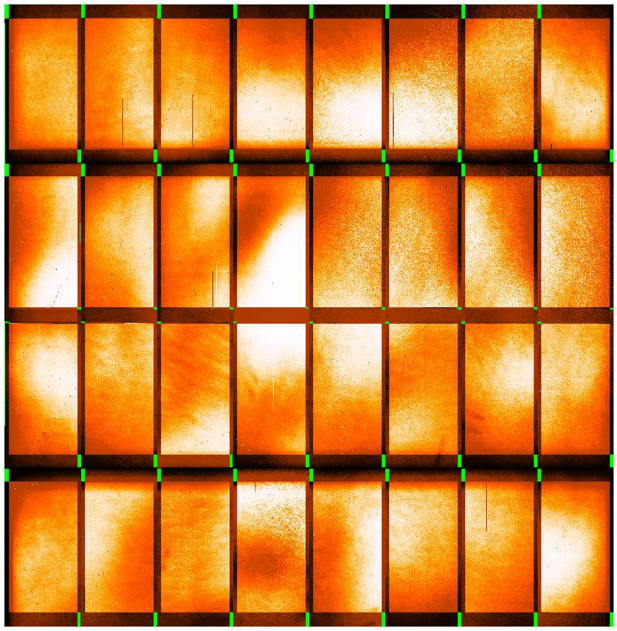

Figure 4. Typical ATLAS confidence map for a stacked tile in *r*. Areas left uncovered by the two-pawprint dither are shown in green. Those at the perimeter of the tile area will be covered by the 2 arcmin tile overlaps.

extension for each of the 32 OmegaCAM CCDs in the stacked tile. Individual CCDs originally contained 2048 × 4096 pixels and the stacked pawprint extensions contain ≈2165 × 4498 pixels to cover the two 25 × 85 arcsec offset CCDs that make up each extension in a stack. This leaves ≈5 arcsec overlaps between the stacked pawprints in each direction where objects can be recorded twice. Along with the imaging data, statistical confidence maps in the same format are also supplied (Irwin et al. 2004). In Fig. 4, we show a typical confidence map from the *r* band. The main 'bar-like' pattern seen is due

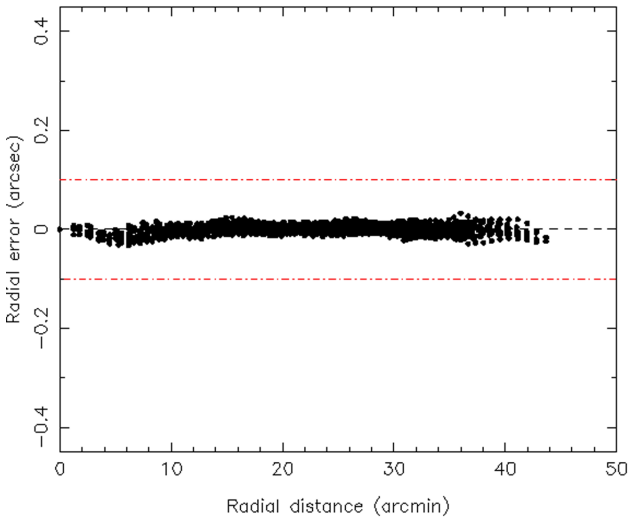

Figure 5. ATLAS astrometric accuracy from 2MASS comparison, as a function of radial distance from the centre of the detector. The red dashed lines represent reference levels of ±100 mas astrometric accuracy.

to the interchip gaps and the dither pattern used to cover them. Note that these are detector-level normalized confidence maps whereby each detector's map is normalized to a median level of 100 per cent, hence the particular shape of the repeating pattern.

Object detection is then carried out to an isophotal limit set to 1.25σ, where σ is a robust (rms) estimate of the average pixel noise over the frame. Catalogues are then produced for the stacked and unstacked images. Aperture, Petrosian and Kron magnitudes are supplied in the first instance along with many other parameters (see Section 2.6 below).

2.3 Astrometry

Astrometric calibration is via the numerous unsaturated 2MASS point sources available in each field. The full two-dimensional astrometric distortion pattern is computed by averaging a series (typically one month of data) of astrometric solution residuals on a regular standard coordinate (ξ, η) grid with spacing of 1 arcmin. The radial distortion points shown in Fig. 5 are the average ξ, η errors for each bin projected along the radial direction. The individual detector astrometric solutions achieve rms accuracies of around 70–80 mas per star – generally dominated by rms errors in 2MASS stars. Even at high Galactic latitudes there are sufficient calibrators to give systematic residuals at the 25 mas level per detector. The global systematics from stacking multiple solutions are better than this as can be seen in Fig. 5. A tangent plane projection is being used for all data products.

2.4 Illumination correction

The open nature of the VST dome provides excellent through-flow of air improving the seeing by reducing the contribution from the dome. However, this also leads to increased scattered light which impairs flat-fielding. In particular an ≈0.2 mag centre to the edge gradient in the photometry is seen from the pawprint. An illumination correction therefore has to be applied to the photometry and this has been done via the AAVSO Photometric All-Sky Survey (APASS) survey (http://www.aavso.org/apass). The APASS survey

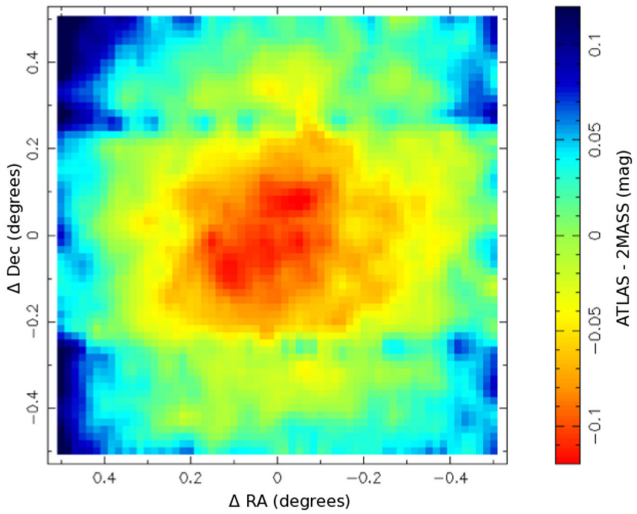

Figure 6. ATLAS illumination correction. ATLAS *i*-band observations processed using the same master flats for the period 2012 August 16 to September 30 and the resulting residuals from the 2MASS photometric catalogue stacked over several hundred independent pointings. The *i*-band colour equations are $i = J + (J - K)*1.175 + 0.459$ (for $H - K \leq 0.15$) and $i = J + (J - K)*1.175 + 0.459 + (H - K - 0.15)*3.529$ (for $H - K > 0.15$).

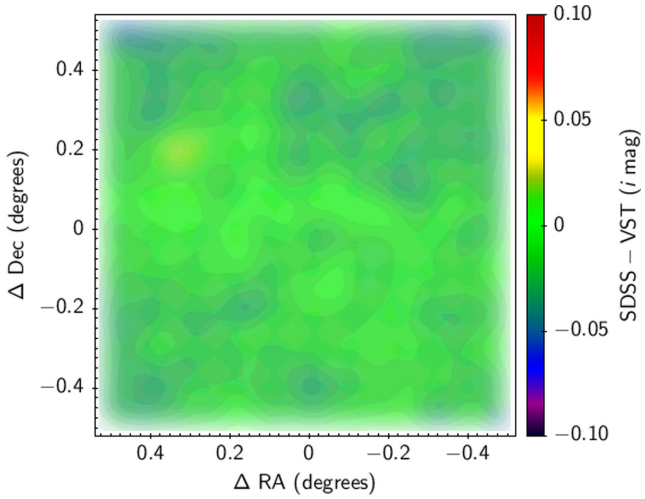

Figure 7. SDSS − ATLAS stellar residuals in *i* from a 10-field stack after ATLAS illumination correction.

is a $g < 16$ mag stellar survey made in the *BVgri* bands. The illumination corrections are obtained from direct, stacked, comparisons between ATLAS and APASS stellar magnitudes for *gri* and from extrapolating APASS *gri* to provide the *u* and *z* corrections. The pattern of residuals across the tile typically looks like that shown in Fig. 6. The scattered light is made up of multiple components having different symmetries and scales causing effects ranging in scale from 10 arcsec with $x - y$ rectangular symmetry, e.g. due to scattering off masking strips of CCDs, to large fractions of the field due to radial concentration in the optics and to non-astronomical scattered light entering obliquely in flats. The illumination correction removes the dominant reproducible components of this effect in the source lists leaving the zero-point across the field uniform to $\approx\pm$ 0.007 mag. ESO have made various attempts to improve the baffling, the latest being in 2014 April, which have reduced the problem by about a factor of 2 over that seen in Fig. 6, but not entirely eliminated it. The illumination correction is updated as necessary to reflect these changes.

We can test the illumination corrections in the overlap area with SDSS. Fig. 7 shows SDSS − ATLAS residuals from a stack of 10 ATLAS *i*-band tiles in the overlap area. The amplitude of the radial pattern of residuals is much reduced from that shown in Fig. 6.

2.5 ATLAS zero-point calibration

The original zero-point calibration was based on the ESO nightly standards in all bands and these were used to place the VST magnitudes for each tile on a Vega-like system. We refer to this as ATLAS(ESO). These standards are observed in any photometric conditions and so cloud can introduce zero-point error. However, due to the excellence of the Paranal site and the clear conditions specified for ATLAS observations, there appears to be a reasonable consistency between the zero-points in night-to-night comparisons. So these ESO standard zero-points make a good first-order calibration of the survey. But in making stellar colour–colour diagrams Chehade et al. (in preparation) found that the stellar locus moved on a regular basis, presumably due to non-photometric conditions in one of the bands between survey field and standard star. Therefore, there is a need for an improved global calibration for ATLAS and we have thus made a first iteration towards a global calibration via APASS.

We used APASS to measure new magnitude zero-points based on a tile-by-tile comparison of unsaturated $g < 16$ mag stars in each ATLAS *gri* tile. In the *u* and *z* bands where there are no APASS data, we again extrapolated from the APASS *gri* bands band to produce the *u* and *z* calibrations. In APASS, the average star sky density is $\approx$100 deg^{-2} although at high latitudes, the star density may be lower. Therefore to improve the statistics we have implemented a nightly ATLAS zero-point based on all the APASS standards observed that night. This also has the effect of averaging out any APASS systematic in an individual ATLAS field. We now assume this nightly zero-point as our default calibration, referred to subsequently as ATLAS(APASS). This calibration can be checked in the SDSS subareas and we will report on the results of this check in Section 4.2.

Note that despite the fact that the original ESO zero-points are in the Vega magnitude system, APASS uses the AB system and so the default for this paper is that the magnitudes are on the APASS AB system unless explicitly stated otherwise. The AB − Vega magnitude offsets were computed to be 0.894 (*u*), −0.100 (*g*), 0.159 (*r*), 0.356 (*i*), 0.517 (*z*). These were calculated for VST telescope and filter throughput and at airmass 1.3 (see Fig. 2) for consistency with SDSS conversions.

We then compared APASS nightly magnitude zero-points with the original ESO zero-points. Fig. 8 shows distributions of the average ATLAS(APASS) − ATLAS(ESO) magnitude zero-point differences on a field-by-field basis over the whole current survey area. We find that the residuals are basically at the $\pm$0.05 mag level but with non-Gaussian tails usually arising from non-photometric conditions. From Fig. 8 we also note that the ATLAS(APASS) − ATLAS(ESO) offsets are in good agreement with the expected offsets except in the case of *u* which has a 0.3 mag discrepancy. It is probable that the *u* band fabricated from APASS *gri* contains a zero-point error and this is confirmed in the comparison with SDSS made in Section 3.2 below. This problem will be corrected at the global calibration stage.

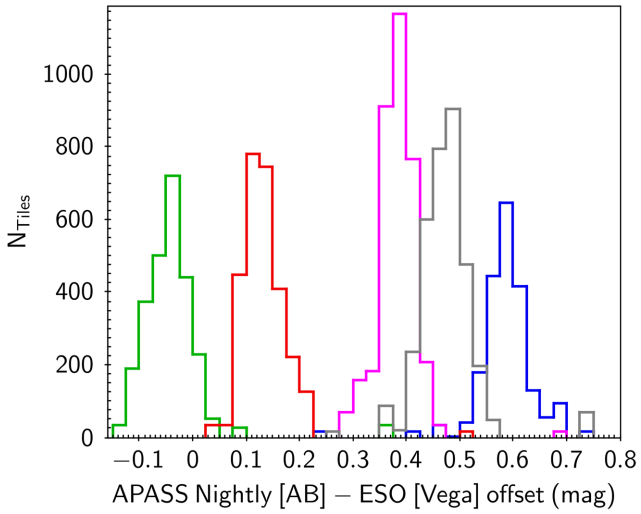

Figure 8. The difference in magnitude zero-points between the ATLAS APASS nightly and ATLAS ESO calibration, averaged on a tile-by-tile basis, over the whole current survey for *u* (blue), *g* (green), *r* (red), *i* (purple), *z* (grey). Here APASS is in AB whereas ESO ATLAS is in the Vega system. The average ATLAS(APASS) − ATLAS(ESO) magnitude offsets and standard deviations are 0.59 ± 0.06 (*u*), -0.042 ± 0.06 (*g*), 0.13 ± 0.045 (*r*), 0.39 ± 0.038 (*i*), 0.47 ± 0.080 (*z*).

2.6 ATLAS photometric parameters

The photometric quantities supplied for ATLAS are Kron and Petrosian pseudo-total magnitudes along with their respective radii. Kron and Petrosian magnitudes are measured in these radii multiplied by a factor of 2. Aperture magnitudes are also given with radii of $1/2 \times r_{\rm core}$, $1/\mathrm{sqrt}(2) \times r_{\rm core}$, $r_{\rm core}$, $\mathrm{sqrt}(2) \times r_{\rm core}$, $2 \times r_{\rm core}$, $2\mathrm{sqrt}(2) \times r_{\rm core}$, $4 \times r_{\rm core}$, $5 \times r_{\rm core}$, $6 \times r_{\rm core}$, $7 \times r_{\rm core}$ where $r_{\rm core} = 1$ arcsec and is the radius of aperture 3. Corrections to total magnitudes for the aperture magnitudes of point sources are also supplied. The Kron, Petrosian and aperture magnitudes for both point sources and extended objects are deblended of overlapping sources. Areal profiles are given as the number of pixels above eight thresholds. Star–galaxy separation statistics, peak heights, sky levels and sky variance are also calculated. A number of other parameters are given and a full list is available at http://casu.ast.cam.ac.uk/surveys-projects/vst/technical/catalogue-generation

2.7 Survey statistics

The seeing distributions by passband are shown in Fig. 9. These show that the median seeing from the CASU measurements is sub-arcsecond in the *riz* bands, and even at *ug* only rises to ≈1 arcsec FWHM. The individual median seeings in each band are given in Table 1. These are significant improvements over median SDSS seeing values e.g. 1.24 arcsec FWHM in *r* (Bramich & Freudling 2012). The distribution of ATLAS(APASS) limiting magnitudes at the 5σ detection level by passband is shown in Fig. 10. The median 5σ stellar magnitude limit in a 1-arcsec radius aperture reaches $r \approx 22.7$. The median limits in all bands are also given in Table 1, where, in order to facilitate comparison with SDSS, we have used the transformations in Section 3.2 to place our magnitudes on the SDSS system. Also given there are ATLAS median magnitude limits calculated in apertures of radius the SDSS FWHM seeing ('ATLAS mag. limit (gal)') and these might be thought more comparable to

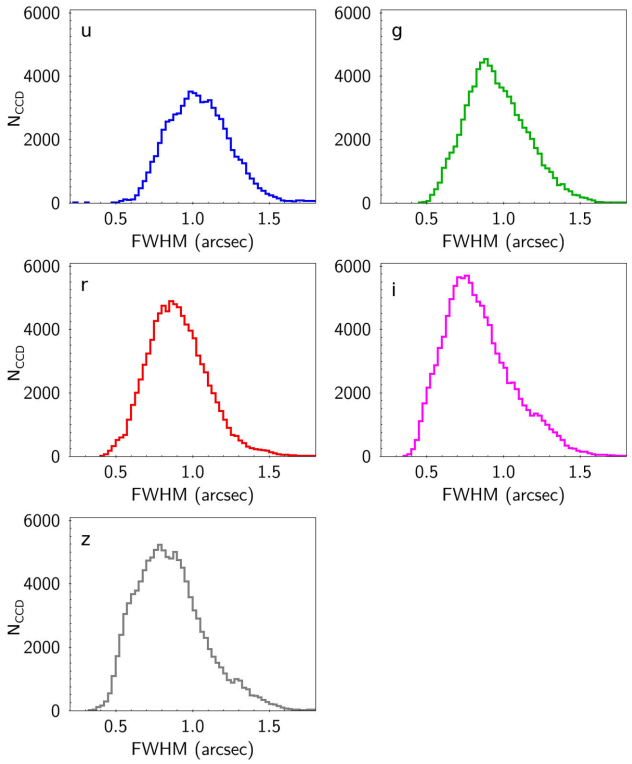

Figure 9. ATLAS FWHM seeing distributions in arcseconds. These are for ESO A and B grade stacked tiles.

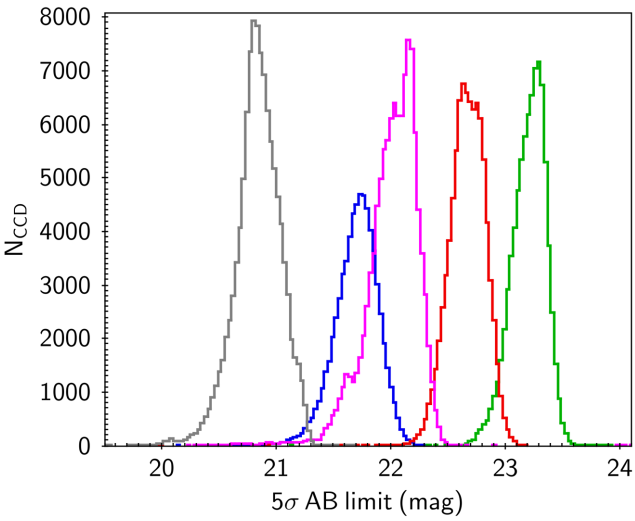

Figure 10. ATLAS(APASS) 5σ AB magnitude limit distributions for point sources in *u* (blue), *g* (green), *r* (red), *i* (purple) and *z* (grey). The median magnitude limits are given in Table 1 where they are compared to the equivalent SDSS limits, allowing for the transformations in Section 3.2.

faint galaxy S/N limits. In Fig. 11, we similarly show the distribution of sky brightnesses and the medians are again given in Table 1. Finally, in Table 1, we also present the count rate in each ATLAS passband for a 20 mag (AB) point source based on the magnitude zero-points.

In Table 1, we also present SDSS statistics for comparison, including seeing, sky brightness and count rates. SDSS seeing

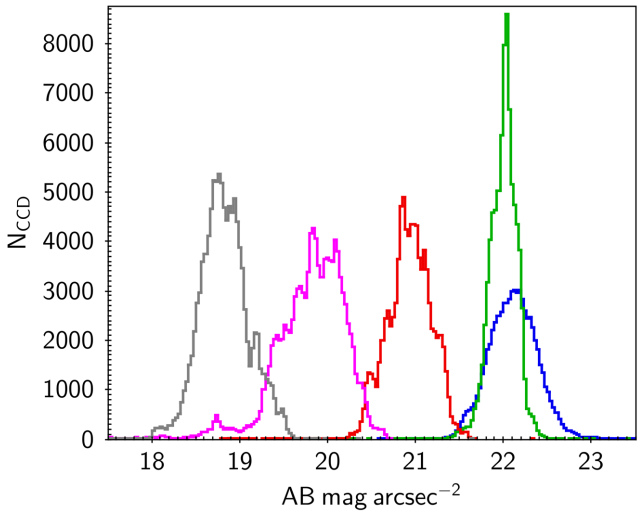

Figure 11. ATLAS(APASS) sky brightness distributions in u (blue), g (green), r (red), i (purple) and z (grey). The median sky brightnesses are given in Table 1 where they are compared to their SDSS equivalents.

statistics are taken from Bramich & Freudling (2012) and sky brightness statistics are sourced from http://www.sdss2.org/dr7/. As already noted, in all bands median ATLAS seeing is significantly better than that of SDSS. Comparing SDSS and ATLAS median sky brightnesses we note that the ATLAS sky brightnesses are fainter than SDSS in u, g, r and slightly brighter in i and z due to ATLAS using greyer conditions for i, z. The SDSS count rates are also given from Stoughton et al. (2002) equation (1) assuming airmass 1.3, as are the quoted ATLAS count rates. We see that the ATLAS and SDSS count rates are similar with ATLAS having a significant advantage only at z, the same conclusion as from the throughput comparison in Fig. 2. The SDSS magnitude limits have been calculated assuming these SDSS count rates and sky brightnesses. They are again 5σ limits for point sources but now measured in the radius of the quoted SDSS seeing (i.e. $\theta < 1.46$ arcsec in u). This means that the ATLAS limits are ≈0.25 mag fainter in *ugri* due to better seeing and 0.7 mag fainter in z, with this extra advantage due to ATLAS's higher throughput in the z band. The comparison of these limits is more favourable to SDSS when the bigger apertures are used to compute ATLAS 5σ limits (mag. limit. (gal)). These are more like the apertures appropriate for faint ATLAS galaxies. Here ATLAS is within 0.15 mag of the SDSS limit in *ugrz* but ATLAS has a 0.31 mag disadvantage in i partly due to a brighter sky brightness (the ATLAS i and z data are mostly taken in grey time, when the moon is up, whereas SDSS used dark time, due to their requirement to observe all five bands simultaneously). Note that ATLAS is sky noise limited in *griz* and read-out-noise limited in u. We conclude that SDSS and ATLAS appear to have comparable magnitude limits for galaxy photometry but that ATLAS has significantly fainter limits than SDSS for stellar photometry mainly due to its better seeing.

3 PHOTOMETRIC SCALES AND COLOUR EQUATIONS

3.1 ATLAS-Vega colour equations

As noted above, the original photometric calibration (as used in ATLAS DR1) was based on the limited number of standard fields observed on most nights. This 'ESO' calibration is in a VST Vega-like system and remains available as an alternative calibration, despite the known issue with occasional non-photometric conditions. Nevertheless, we list below the linear colour equations used to convert the standards to an internal VST system for the ESO Vega calibration:

$$u_{\rm VST} = U + 0.035(U - B) \quad (1)$$

$$g_{\rm VST} = B - 0.405(B - V) \quad (2)$$

$$r_{\rm VST} = R + 0.255(V - R) \quad (3)$$

$$i_{\rm VST} = I + 0.115(R - I) \quad (4)$$

$$z_{\rm VST} = I - 0.390(R - I). \quad (5)$$

As noted in Section 2.5, we have since re-calculated all the zero-points based now on the illumination-correction fixed catalogues while computing APASS AB nightly and field-by-field magnitude zero-points.

3.2 ATLAS–SDSS colour equations

In the equatorial regions there is an ≈300 deg^2 overlap with SDSS, split between the SGC (≈180 deg^2) and the NGC (≈120 deg^2). In the SGC the overlap is at RA ≈ $22^{\rm h}40^{\rm m}$–$03^{\rm h}$, $-11^\circ <$ Dec $< -9^\circ$ and in the NGC it is at RA ≈ $10^{\rm h}00^{\rm m}$–$15^{\rm h}30^{\rm m}$, $-3.5^\circ <$ Dec $< -2^\circ$. We have compared *ugriz* (AB) colours of SDSS and ATLAS(APASS) stars in the 120 deg^2 NGC overlap region to define the colour equations between the two systems. We use PSF magnitudes for SDSS and aperture 3 (corrected to total) magnitudes for ATLAS. The magnitude ranges used are $14 < u < 20$, $15 < g < 20$, $15 < r < 20$, $14 < i < 19$ and $13.5 < z < 18.5$.

In Fig. 12, we show $u_{\rm SDSS} - u$: $u - g$, $g_{\rm SDSS} - g$: $g - r$, $r_{\rm SDSS} - r$: $g - r$, $i_{\rm SDSS} - i$: $r - i$, $z_{\rm SDSS} - z$: $i - z$. We see that the colour terms

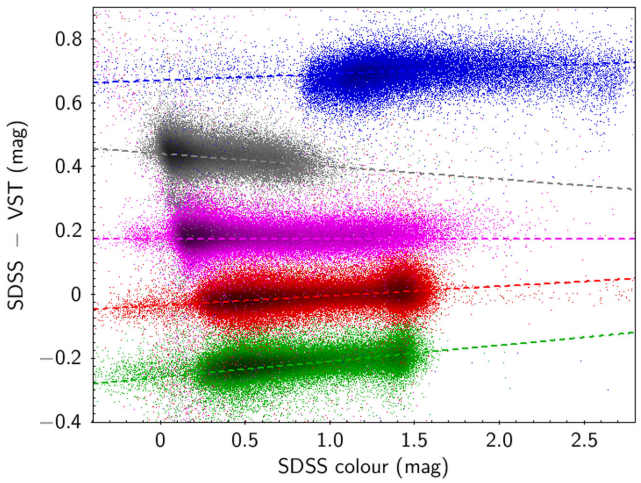

Figure 12. Colour equations between ATLAS(APASS) aperture 3 magnitudes and SDSS PSF magnitudes for stars in $u_{\rm SDSS} - u$ versus $(u - g)_{\rm SDSS}$ (blue), $g_{\rm SDSS} - g$ versus $(g - r)_{\rm SDSS}$ (green), $r_{\rm SDSS} - r$ versus $(g - r)_{\rm SDSS}$ (red), $i_{\rm SDSS} - i$ versus $(r - i)_{\rm SDSS}$ (purple) and $z_{\rm SDSS} - z$ versus $(i - z)_{\rm SDSS}$ (grey). ATLAS(APASS) magnitudes are derived from the APASS nightly zero-points. The points have been displaced in the ordinate for clarity, $g_{\rm SDSS} - g$ by −0.2, $i_{\rm SDSS} - i$ by +0.2, $z_{\rm SDSS} - z$ by +0.4 and $u_{\rm SDSS} - u$ by +0.4. Apart from this, the dashed lines are the equations given in Section 3.2.

in u and i are almost negligible but there are small colour terms in grz. We find that

$$u_{\rm SDSS} = u_{\rm VST} + 0.01(u-g)_{\rm SDSS} + 0.27 \quad (6)$$

$$g_{\rm SDSS} = g_{\rm VST} + 0.05(g-r)_{\rm SDSS} - 0.06 \quad (7)$$

$$r_{\rm SDSS} = r_{\rm VST} + 0.03(g-r)_{\rm SDSS} - 0.035 \quad (8)$$

$$i_{\rm SDSS} = i_{\rm VST} - 0.025 \quad (9)$$

$$z_{\rm SDSS} = z_{\rm VST} - 0.04(i-z)_{\rm SDSS} + 0.04. \quad (10)$$

We note that the zero-point offsets with SDSS are small and due to slight differences in effective bandpass wavelengths. The exception is u where the ATLAS(APASS) AB zero-points had to be fabricated from APASS gri. This is due to the non-linear (even double-valued for some star types) transformation really required when going from g, r to u. We have investigated if these offsets are caused by the method of magnitude measurement and find that these results are robust. Note that this issue in u does not affect the AB magnitudes in Table 1 and Figs 8, 10 and 11 since these are based on the original ESO Vega calibration plus the computed AB − Vega offsets given in Section 2.5.

We find good agreement in the colour coefficients with the SDSS - VST gri band conversions independently reported by the KiDS team at http://kids.strw.leidenuniv.nl/DR1/images/cterms.png as

$$g_{\rm SDSS} = g_{\rm VST} + 0.0522(g-r)_{\rm SDSS} \quad (11)$$

$$r_{\rm SDSS} = r_{\rm VST} + 0.0321(g-r)_{\rm SDSS} \quad (12)$$

$$i_{\rm SDSS} = i_{\rm VST} + 0.0155(r-i)_{\rm SDSS}. \quad (13)$$

Typical extinction coefficients (mag) for ATLAS are 0.46(u), 0.19(g), 0.09(r), 0.05(i), 0.05(z).

3.3 ATLAS-SDSS comparison

We next compare linearity of the ATLAS(APASS) photometry (after the above colour corrections), with SDSS in the ≈120 deg^2 NGC overlap area. We shall see later that there are still some area-dependent zero-point problems with the ATLAS(APASS) calibrations but here we will focus on the r-band where the field-field problems are less. In the top panel of Fig. 13, we plot ATLAS(APASS) aperture magnitudes versus model magnitudes for SDSS stars. The relation is consistent with linearity over the full $13 < r < 22.5$ mag range. In the middle panel of Fig. 13, we plot ATLAS(APASS) Kron magnitudes against SDSS model magnitudes for galaxies. An offset to total of −0.15 mag for galaxies is suggested for ATLAS. The relation appears noisier than the stars as expected but with no evidence of a scale error to $r \approx 22$. In the bottom panel of Fig. 13, we similarly plot ATLAS Petrosian magnitudes for galaxies against model magnitudes for SDSS. We see a reasonably linear, if noisier, relation. In the $22 < r < 22.5$ bin, the rms error reaches ±0.2, ±0.38 and ±0.38 mag for aperture, Petrosian and Kron magnitudes, and here we might expect roughly equal contributions from ATLAS and SDSS. Overall, for VST ATLAS, we therefore recommend that aperture magnitudes (aperture 3) are used for stars while Petrosian or Kron magnitudes are used for galaxies.

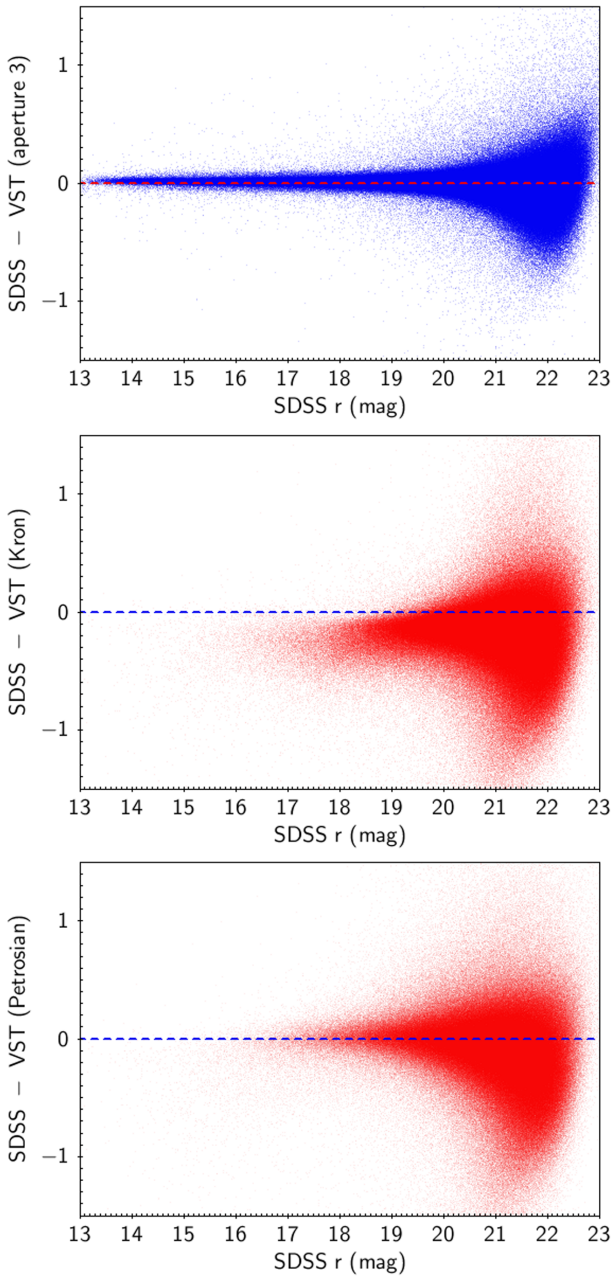

Figure 13. SDSS NGC overlap comparisons of ATLAS(APASS) aperture (corrected to total), Kron and Petrosian AB magnitudes (corrected for colour terms as in Section 3.2) for stars (blue) and galaxies (red) with SDSS model magnitudes in both cases. No corrections to total magnitudes have been applied to the Kron and Petrosian magnitudes.

These results for the r band are typical of the results for the other four bands. These can be found at http://astro.dur.ac.uk/Cosmology/vstatlas/tests/.

3.4 ATLAS–Stripe 82 (WHDF field) comparison

Because SDSS only reaches a similar depth to ATLAS, it is not clear which survey is dominating the error spread at faint magnitudes. We have therefore also compared ATLAS photometry for galaxies and stars with the much deeper Stripe 82 photometry which lies within a 1 deg^2, specially observed, ATLAS area which also

Table 2. ATLAS WHDF field seeing, 5σ point source magnitude limits and sky brightnesses, compared to ATLAS median parameters from Table 1. All magnitudes are quoted in the AB system.

Band	*u*	*g*	*r*	*i*	*z*
WHDF exposure (s)	2 × 60	2 × 50	2 × 45	2 × 45	2 × 45
WHDF airmass	1.52	1.46	1.16	1.14	1.13
WHDF seeing (arcsec)	1.27	1.36	1.04	0.99	1.06
ATLAS median seeing (arcsec)	1.02	0.95	0.90	0.81	0.84
WHDF mag. limit	21.45	22.50	22.46	21.85	20.65
ATLAS median mag. limit	21.99	23.14	22.67	21.99	20.87
WHDF sky brightness	21.56	21.64	20.77	19.96	18.80
ATLAS median sky brightness	22.34	21.90	20.92	19.78	18.85

contains the William Herschel Deep Field (WHDF; Metcalfe et al. 2006) and again its deeper multi-epoch photometry allows a comparison to check the magnitude dependent error of the ATLAS photometry.

We note that although the WHDF ATLAS data have the same exposure as the ATLAS survey data and were taken in dark time, the seeing particularly in *u* and *g* is significantly worse than average (see Table 2). Indeed, the 5σ point source magnitude limits in all bands are brighter than the ATLAS average from ≈0.2 mag in *riz*, to 0.64 mag in *g* and 0.54 mag in *u* (see Table 2). Nevertheless we can still make approximate checks of these brighter than usual WHDF ATLAS mag limits by comparison to deeper Stripe 82 data.

So in Fig. 14 we now show in the top panel the comparison between Stripe 82 model magnitudes and ATLAS aperture 3 magnitudes for point sources. Again the relation is linear with a low dispersion of ±0.15 mag at the 5σ WHDF ATLAS limit of $r = 22.46$ from Table 2. Indeed, ATLAS aperture magnitudes in all bands show good agreement with the Stripe 82 magnitudes to their respective 5σ limits from Table 2, confirming that the accuracy of these limits for point sources (see http://astro.dur.ac.uk/Cosmology/vstatlas/tests). The middle and bottom panels show the comparison between Stripe 82 model magnitudes and ATLAS Petrosian/Kron magnitudes now for SDSS galaxies. Both Petrosian and Kron magnitudes are reasonably linear but Petrosian appears to have a higher dispersion at $r \approx 21.5$ of ±0.2 mag as opposed to ±0.15 mag for Kron. On this basis the preferred ATLAS magnitude for galaxy photometry again appears to be Kron magnitudes.

4 ZERO-POINT COMPARISONS WITH APASS AND SDSS

4.1 APASS versus ATLAS

We now move away from checks of the linearity of ATLAS photometry to address in more detail the question of the consistency of the ATLAS zero-point calibration as discussed in Section 2.5 over wider areas of the survey. Maps of APASS − ATLAS(ESO) residuals for individual stars in an ≈300 deg^2 area centred on RA ≈ 23^h, Dec ≈ −30° are shown in Fig. 15. The ATLAS data are calibrated from the ESO standards as used for the DR1 data release. The offsets in *u* are obtained by extrapolating to *u* from APASS *B*, *V* and the *z* offsets are from interpolating APASS *r* and *i* measurements. Offsets are seen that are clearly due to ATLAS(ESO) calibration issues (generally in blocks of ∼17 × 1 deg, corresponding to a single concatenation of tiles). Clearly some within field residuals are seen, particularly in *i* (and *z*), that do not show any ATLAS characteristics and we believe that these may be due to problems in the APASS *i*-band (and its extrapolation to *z*). The distribution of ATLAS(APASS) − ATLAS(ESO) (tile-by-tile) residuals for *ugriz* over a larger area is shown in Fig. 8 and the standard deviations are ±0.060 mag (*u*), ±0.060 mag (*g*), ±0.045 mag (*r*), ±0.038 mag (*i*), ±0.080 mag (*z*).

4.2 ATLAS–SDSS equatorial comparison

Figs 16–20 show the residuals between the SDSS data for stars in the NGC overlap area at $10^h < RA < 15^h30^m$ and $-3.^\circ5 < Dec < -2^\circ$ assuming, in turn, the ATLAS(ESO) calibration and the ATLAS(APASS) calibration. The SDSS magnitude ranges used are $14 < u < 20$, $15 < g < 20$, $15 < r < 20$, $14 < i < 19$ and $13.5 < z < 18.5$. The standard SDSS calibration was used here for simplicity, rather than the uber-calibration of Padmanabhan et al. (2008). As with the APASS comparison in Section 4.1, the ESO calibration clearly shows ±0.05 mag offsets on the scale of single concatenations. These are effectively removed by using the APASS nightly calibration. The ESO calibration also has larger residuals with clear VST nightly correlations. Some nights have no useable ESO standards and on these a long-term average default value is used, perhaps explaining some of the stripes. However, even the APASS nightly calibration still has occasional issues with individual fields as can be seen in the *z*-band image. Also, we already noted that the APASS *i* (and *z*) band photometry still has some issue from the APASS − ATLAS(ESO) comparison above.

The distributions of the mean tile-by-tile SDSS − ATLAS residuals (for stars) in *ugriz* for the ATLAS(ESO) and ATLAS(APASS) calibrations are compared in Fig. 21. For clarity, the ATLAS(ESO) residuals have been corrected to AB using the offsets given in Section 2.5. We measure on a tile-by-tile basis to reduce the effect of individual star random errors (a typical tile has between a few hundred and a few thousand stars contributing to the mean). Generally, the APASS nightly calibrated data give the smallest scatter with SDSS. The ESO calibration, and the APASS individual tile calibration (not shown, but see Section 2.5), appear to give larger scatter, in the latter case presumably due to statistical errors with the calibration based on fewer APASS stars. The ATLAS(APASS) − SDSS magnitude standard deviations are ±0.035, ±0.013, ±0.013, ±0.012 and ±0.055 mag in *ugriz*, in most bands a significant improvement over the ATLAS(ESO)–SDSS comparison (±0.045, ±0.027, ±0.037,

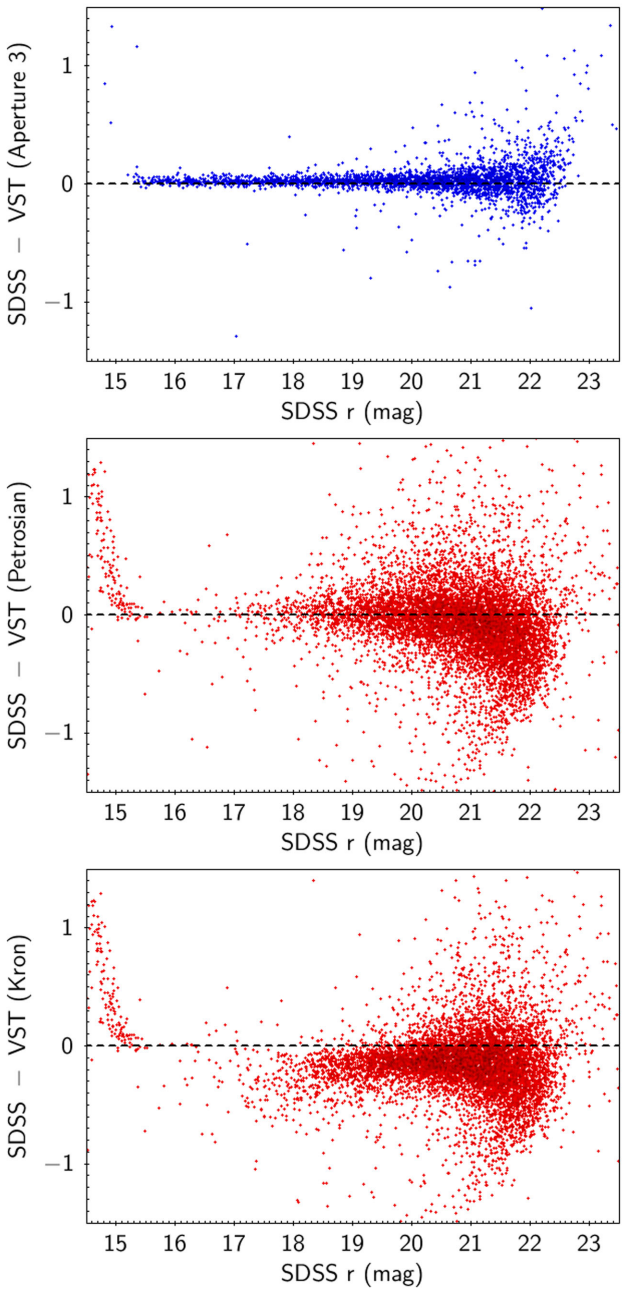

Figure 14. Top: SDSS Stripe 82 model magnitude–ATLAS aperture magnitude *r*-band comparison in the WHDF field for stars (blue). Middle: same comparison now based on ATLAS Petrosian magnitudes for galaxies (red). Bottom: same comparison now based on ATLAS Kron magnitudes for galaxies (red). In the two lower panels, saturation in Stripe 82 magnitudes of misclassified stars causes the non-linearity at $r < 15.5$.

± 0.035 and ± 0.073 in *ugriz*). These standard deviations were measured on the basis of 183 tiles in *griz* and 112 tiles in *u*. In both cases, the *z*-band result is affected by the presence of a single tile whose average is 0.66 mag offset from the mean. Nevertheless, in all bands the improvement gained from the APASS nightly calibration is clear.

For the final release, we are currently investigating several global calibration methods including the matrix inversion technique (Glazebrook et al. 1994), which relies on the 2 arcmin overlaps between fields, and the stellar locus regression technique (High et al. 2009).

4.3 Star–galaxy separation comparisons

We now use the same NGC SDSS DR9 overlap area to compare ATLAS star–galaxy separation with that of SDSS. The results are shown in Fig. 22. Comparing top-left and top-right panels in the ATLAS(APASS) Aper3-Petrosian : *g* magnitude star–galaxy separation plane, we see that the ATLAS star–galaxy separation statistic has included some SDSS stars just above the stellar loci shown in the lower panels. These misclassified ATLAS stars have come from areas frequently coinciding with interchip gaps as can be seen in the upper panel of Fig. 23. The problem arises when the image quality varies slightly between the two subexposures and so the stellar locus is offset in the interchip areas when there is only one subexposure contributing to the image. Depending on the direction of the shift, this can result in stars being classified as galaxies. This problem will clearly be present in the ATLAS DR1 data. However, it is easy to fix this problem by plotting Δ VST (Aper3-Petrosian) versus VST Petrosian for ATLAS classified galaxies and then remove the misclassified stars by a magnitude independent cut. This has the effect of cleaning up the misclassified stars as shown in the lower panel of Fig. 23.

5 GALAXY AND STAR NUMBER COUNTS

Adopting the corrected star–galaxy classifier, we next calculate the galaxy (and star) counts from 250 deg^2 in the $-40^\circ <$ Dec $< -25^\circ$ range in the SGC which includes the South Galactic Pole (SGP). Previously 2MASS counts have suggested evidence for a local underdensity in the SGP region. Here we simply focus on the counts to use their turnover to indicate the rough completeness limits of the survey. In Fig. 24, we compare these to a variety of previous galaxy counts compiled by Metcalfe et al. (2001). 2MASS counts suggest evidence for a local underdensity in the SGP region (Whitbourn & Shanks 2014) but a fuller investigation of this issue using ATLAS data in a bigger area will be presented by Mackenzie et al. (in preparation). We see that the galaxy counts agree very well in most bands with other authors until the counts turn over due to incompleteness at faint magnitudes. This happens at AB mag $u \approx 20$, $g \approx 22.5$, $r \approx 22$, $i \approx 21$ and $z \approx 20$. These are in reasonable agreement with the mag. limit (gal) 5σ limits for ATLAS given in Table 1. Star counts turn over at about the same limits but this is more dictated by the star–galaxy separation algorithm and is less related to more fundamental signal-to-noise considerations.

6 ACCESS TO ATLAS DATA

The ESO Science Archive provides a repository for data products released by the ESO Public Survey teams. Images and catalogues from ATLAS Data Release 1 can be retrieved from http://archive.eso.org/wdb/wdb/adp/phase3_main/form?phase3_collection=ATLAS&release_tag=1.

ATLAS data are also available through the OmegaCAM Science Archive (OSA, http://osa.roe.ac.uk), curated by the Wide-Field Astronomy Unit (WFAU) at the University of Edinburgh. Similar in design to the science archives developed by WFAU for sky survey data from UKIRT/WFCAM (Hambly et al. 2008) and VISTA (Cross et al. 2012), the OSA provides a range of access methods to both image and catalogue data products. It stores ATLAS catalogue data and image metadata in a relational data base management system, which can be queried through the OSA web interface or using the

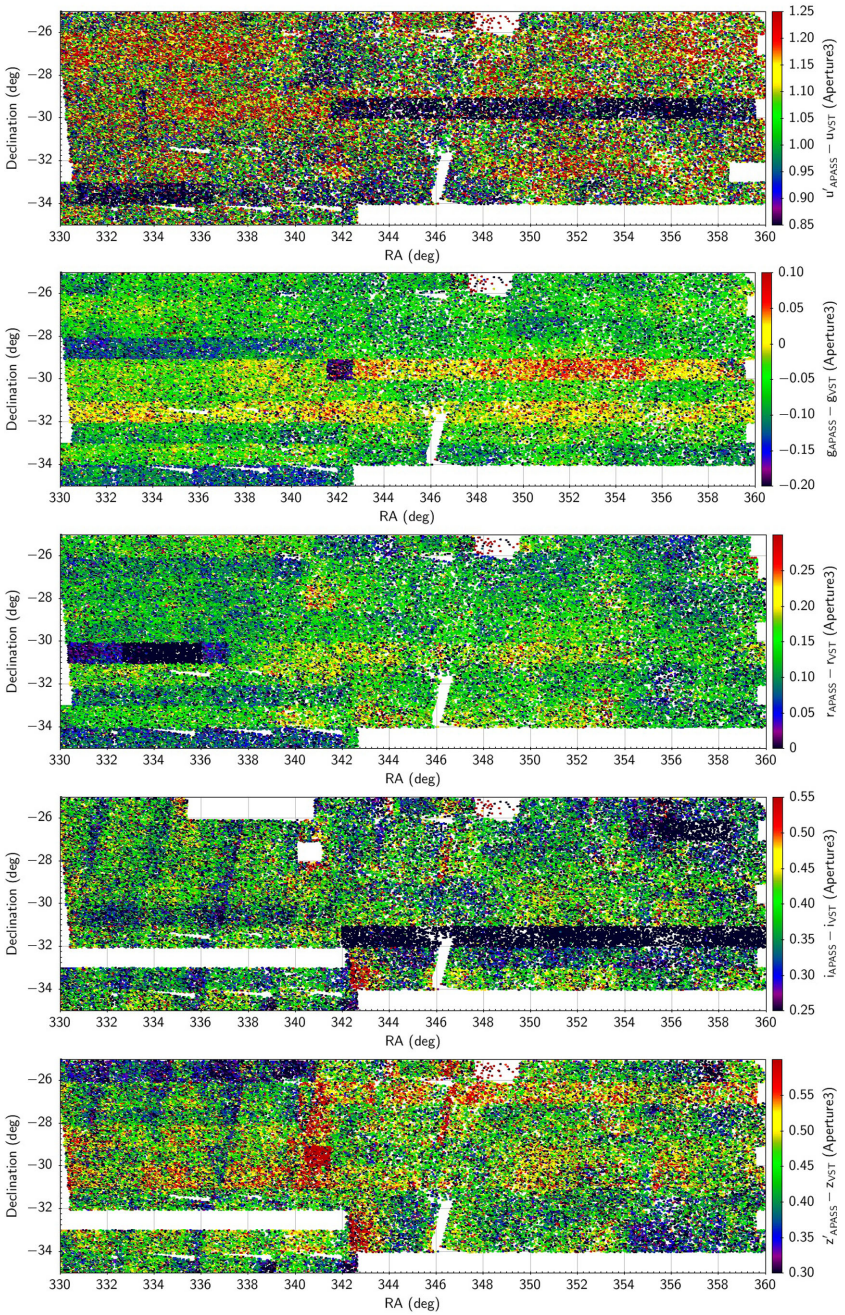

Figure 15. From top to bottom, APASS − ATLAS(ESO) comparisons for stars in *u*, *g*, *r*, *i*, *z*. APASS mag are in AB and ATLAS(ESO) in Vega. These are for ATLAS stacks of ESO A, B grade tiles. Generally, rectangular stripes 1 deg high indicate ATLAS zero-point issues, whereas other features appear to be related to APASS.

Virtual Observatory (VO) Table Access Protocol (Dowler, Rixon & Tody 2011). Query results can be viewed within the OSA web interface or sent directly from it to VO-compliant desktop tools like ALADIN (Bonnarel et al. 2000) and TOPCAT (Taylor 2005), using the Simple Application Message Protocol (Taylor et al. 2012) standard. The OSA also integrates ATLAS catalogue data with a number of sky survey data sets, including SDSS, 2MASS, VHS and *WISE*, and provides the ATLAS consortium with access to proprietary data, as well as supporting use of ATLAS public data releases by the wider astronomical community.

7 CONCLUSIONS

We have described the basic characteristics of VST ATLAS. We find it meets its basic specification of comprising a 'Southern Sloan'. This applies both to the median 5σ mag limits for point sources which are at least as deep as SDSS and to the median sky brightnesses which are comparable to SDSS. But in terms of its spatial resolution, the ATLAS survey presents essentially subarcsecond 0.8–1.0 arcsec median seeing compared to the 1.2–1.5 arcsec median imaging of SDSS.

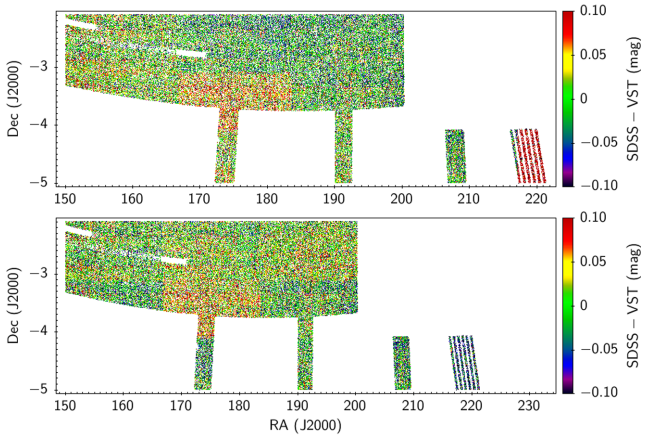

Figure 16. SDSS–ATLAS comparison in *u* with ATLAS(ESO)–SDSS (top) and ATLAS(APASS)–SDSS (bottom). Aperture 3 magnitudes are used for ATLAS and PSF magnitudes for SDSS.

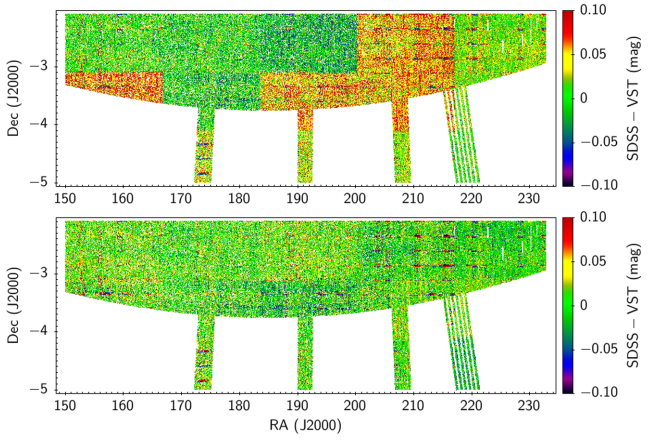

Figure 17. SDSS–ATLAS comparison in *g* with ATLAS(ESO)–SDSS (top) and ATLAS(APASS)–SDSS (bottom). Aperture 3 magnitudes are used for ATLAS and PSF magnitudes for SDSS.

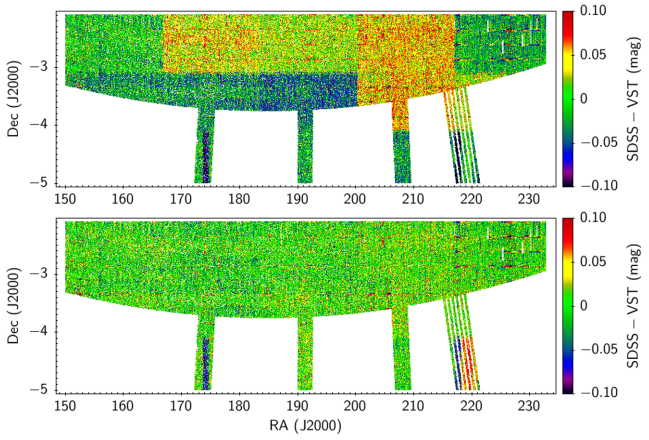

Figure 18. SDSS–ATLAS comparison in *r* with ATLAS(ESO)–SDSS (top) and ATLAS(APASS)–SDSS (bottom). Aperture 3 magnitudes are used for ATLAS and PSF magnitudes for SDSS.

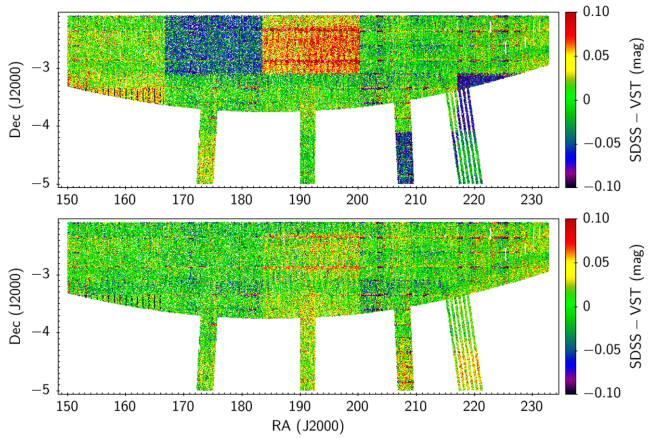

Figure 19. SDSS–ATLAS comparison in *i* with ATLAS(ESO)–SDSS (top) and ATLAS(APASS)–SDSS (bottom). Aperture 3 magnitudes are used for ATLAS and PSF magnitudes for SDSS.

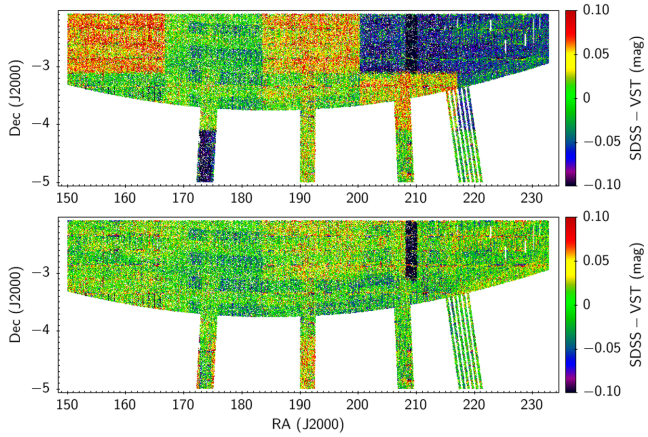

Figure 20. SDSS–ATLAS comparison in *z* with ATLAS(ESO)–SDSS (top) and ATLAS(APASS)–SDSS (bottom). Aperture 3 magnitudes are used for ATLAS and PSF magnitudes for SDSS.

We have derived the colour equations relating ATLAS stellar photometry to SDSS photometry. We find there are small but non-negligible colour terms, particularly in *grz*.

We have demonstrated the linearity of the ATLAS photometry by comparison in the 120 deg^2 NGC overlap area with SDSS. We recommend that 1-arcsec radius (aperture 3) apertures are used for stellar photometry. For galaxies, ATLAS Kron magnitudes seem to give the most linear relations with SDSS model magnitudes. The same conclusions are found by comparing ATLAS and Stripe 82 photometry in the WHDF field. Here we found that the rms dispersions reached ±0.05 mag for stars at $r < 22$ and ±0.15 mag for Kron galaxy magnitudes at $r < 21.5$ mag

The current zero-points assumed for *ugriz* come from APASS stellar photometry applied to nightly blocks of ATLAS data and appear good to $\approx\pm0.02$ mag by comparison with SDSS data in overlap areas. We have investigated how area dependent these zero-points are in the SDSS overlap area and find there are still small areas with residual errors. In the final global calibration,

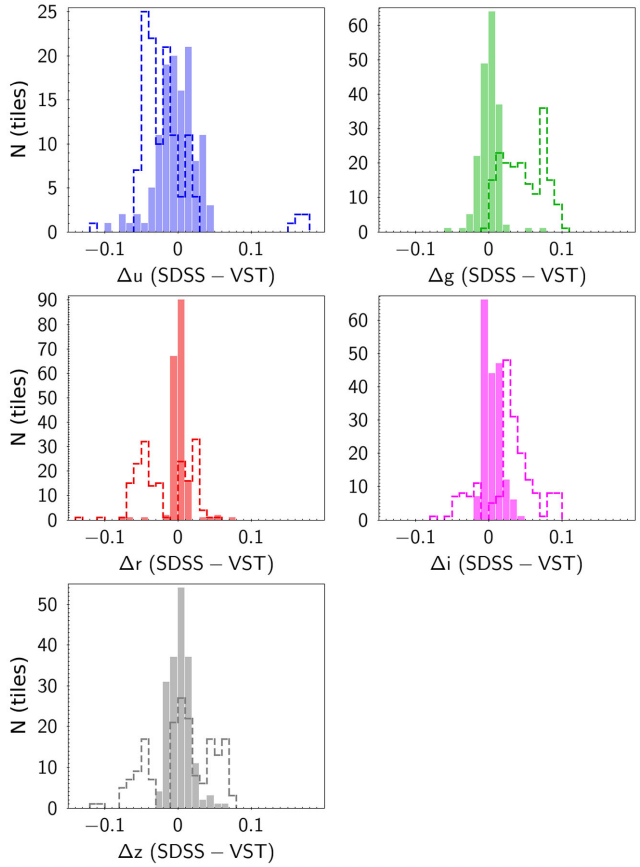

Figure 21. SDSS–ATLAS magnitude residuals for point sources in the SDSS overlap area, averaged on a tile-by-tile basis. The dashed histograms refer to ATLAS(ESO) calibration, the solid histograms refer to ATLAS(APASS) calibration. The magnitude ranges used are $14 < u < 20$, $15 < g < 20$, $15 < r < 20$, $14 < i < 19$ and $13.5 < z < 18.5$. The ATLAS(ESO) data has been corrected to AB using the offsets in Section 2.5.

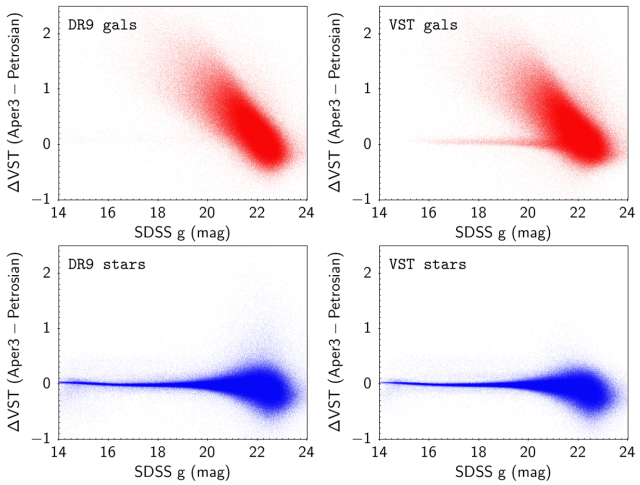

Figure 22. Star–galaxy separation comparison. Left: using the SDSS classifier. Right: using the ATLAS classifier. Upper: galaxies (red). Lower: stars (blue). The thin streak in the upper-right panel is due to stellar objects misclassified as galaxies by the default ATLAS classifier, due to problems in partially covered interchip gaps. All these objects are classified as stellar in SDSS.

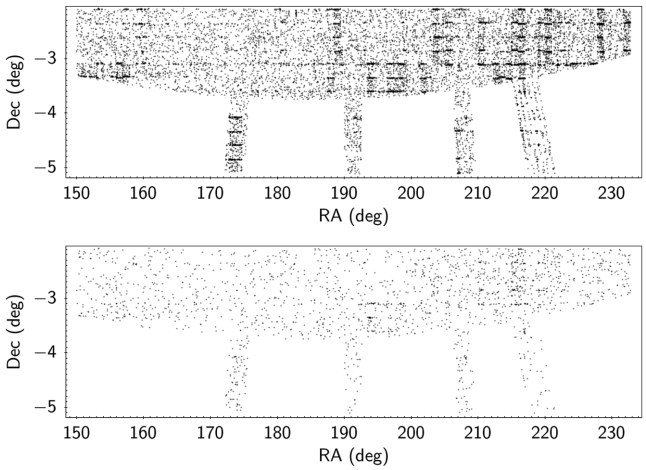

Figure 23. Upper: map showing ATLAS classified galaxies which are stars according to SDSS, down to $g \approx 20.5$. These are found particularly in areas corresponding to interchip gaps. Lower: same as above except the additional star–galaxy separation method described in Section 4.3 has now been applied to the ATLAS galaxies.

we shall use the 2 arcmin overlaps between tiles to reduce these errors.

We have tested the ATLAS star–galaxy separation by comparison with SDSS in the overlap areas and we found that 10 per cent galaxies were misclassified as stars. We also found that 15 per cent stars were misclassified as galaxies and that this higher rate was due to problems occurring in interchip gaps where only one subexposure was available. However, the problem is easily cured by using a more conservative star–galaxy separation line particularly at bright magnitudes.

Finally, we also presented galaxy and star number counts in a 250 deg^2 area at the SGP and found where they turned over to define effective completeness limits. The galaxy counts turn over about at about our quoted 5σ mag limits for galaxies. Star counts turn over at about the same limits but this is mainly dictated by the star–galaxy separation algorithm.

We conclude that the VST ATLAS is ready for scientific analysis. Currently the survey is 75 per cent complete and it should be 100 per cent complete by the end of 2015.

ACKNOWLEDGEMENTS

The ATLAS survey is based on observations made with ESO telescopes at the La Silla Paranal Observatory under programme ID 177.A-3011. We are indebted to the CASU for reducing the ATLAS images and producing catalogues. We also acknowledge the work of the WFAU at Edinburgh for archiving the ATLAS data. WFAU is supported by the Science and Technology Facilities Council grants ST/M001989/1 and ST/M007812/1. We also acknowledge use of publicly available SDSS data. This research has also made use of the APASS data base, located at the AAVSO website. Funding for APASS has been provided by the Robert Martin Ayers Sciences Fund. Work at Durham was supported by the Science and Technology Facilities Council grant ST/L00075X/1. BC would like to acknowledge the support of an STFC studentship.

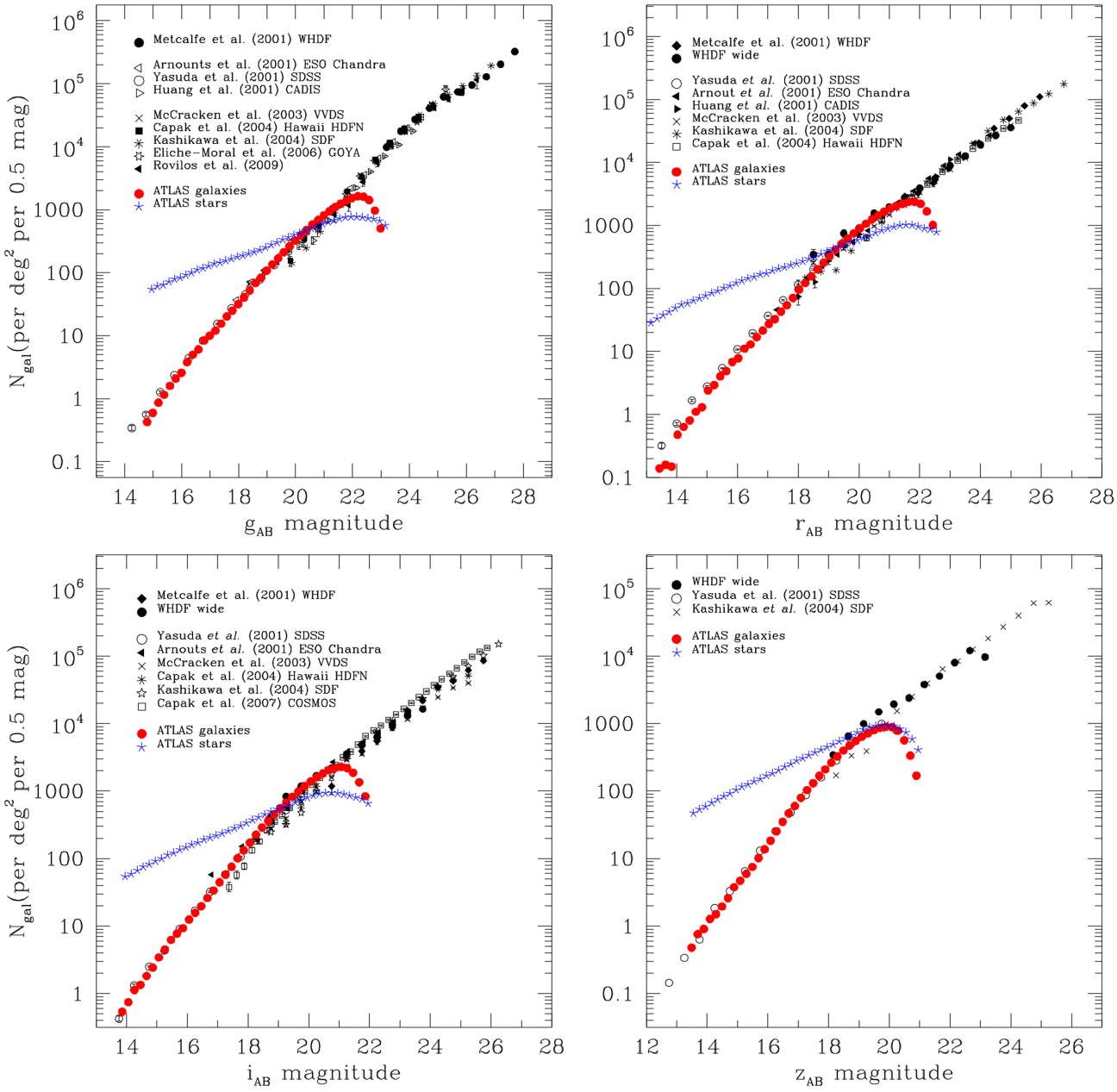

Figure 24. VST ATLAS(APASS) galaxy (red circles) and star (blue stars) counts from a test 250 deg^2 area compared to SDSS and other literature galaxy counts. Both stars and galaxies are measured in Kron magnitudes, brightened by 0.15 mag to take them to total. WHDF wide data are taken from http://astro.dur.ac.uk/∼nm/pubhtml/counts/.

REFERENCES

Arnouts S. et al., 2001, A&A, 379, 740

Belokurov V., Irwin M. J., Koposov S. E., Evans N. W., Gonzalez-Solares E., Metcalfe N., Shanks T., 2014, MNRAS, 441, 2124

Bonnarel F. et al., 2000, A&AS, 143, 33

Bovy J. et al., 2012, ApJ, 749, 41

Bramich D. M., Freudling W., 2012, MNRAS, 424, 1584

Capak P. et al., 2004, AJ, 127, 180

Carnall A. C. et al., 2015, MNRAS, 451, L16

Cross N. J. G. et al., 2012, A&A, 548, A119

de Jong J. T. A. et al., 2013, The Messenger, 154, 44

Dowler P., Rixon G., Tody D., 2011, preprint (arXiv:1110.0497)

Edge A., Sutherland W., Kuijken K., Driver S., McMahon R., Eales S., Emerson J. P., 2013, The Messenger, 154, 32

Eliche-Moral M. C., Balcells M., Prieto M., Garcáa-Dabó C. E., Erwin P., Cristóbal-Hornillos D., 2006, ApJ, 639, 644

Glazebrook K., Peacock J. A., Collins C. A., Miller L., 1994, MNRAS, 266, 65

Goto T. et al., 2002, PASJ, 54, 515

Hambly N. C. et al., 2008, MNRAS, 384, 637

High F. W., Stubbs C. W., Rest A., Stalder B., Challis P., 2009, AJ, 138, 110

Huang J.-S. et al., 2001, A&A, 368, 787

Irwin M. J. et al., 2004, in Quinn P. J., Bridger A., eds, Proc. SPIE Vol. 5493, Optimizing Scientific Return from Astronomy through Information Technologies. SPIE, Bellingham, p. 411

Kashikawa N. et al., 2004, PASJ, 56, 1011

Keenan R. C., Barger A. J., Cowie L. L., 2013, ApJ, 775, 62

Koposov S. E., Irwin M., Belokurov V., Gonzalez-Solares E., Yoldas A. K., Lewis J., Metcalfe N., Shanks T., 2014, MNRAS, 442, L85

Kuijken K. et al, 2011, The Messenger, 146, 8
McCracken H. J. et al., 2003, A&A, 410, 17
McMahon R. G., Banerji M., Gonzalez E., Koposov S. E., Bejar V. J., Lodieu N., Rebolo R., the VHS Collaboration, 2013, The Messenger, 154, 35
Merloni A. et al., 2012, preprint (arXiv:1209.3114)
Metcalfe N., Shanks T., Campos A., McCracken H. J., Fong R., 2001, MNRAS, 323, 795
Metcalfe N., Shanks T., Weilbacher P. M., McCracken H. J., Fong R., Thompson D., 2006, MNRAS, 370, 1257
Mountrichas G., Shanks T., 2007, MNRAS, 380, 113
Padmanabhan N. et al., 2008, ApJ, 674, 1217
Rovilos E. et al., 2009, A&A, 507, 195
Sawangwit U., Shanks T., Cannon R. D., Croom S. M., Ross N. P., Wake D. A., 2010, MNRAS, 402, 2228
Schipani P. et al., 2012, in Stepp L. M., Gilmozzi R., Hall H. J., eds, Proc. SPIE Vol. 8444, Ground-based and Airborne Telescopes IV. SPIE, Bellingham, p. 84441C
Shanks T. et al., 2013, The Messenger, 154, 38
Stoughton C. et al., 2002, AJ, 123, 485
Taylor M. B., 2005, in Shopbell P. L., Britton C. M., Ebert R., eds, ASP Conf. Ser. Vol. 347, Astronomical Data Analysis Software and Systems (ADASS) XIV. Astron. Soc. Pac., San Francisco, p. 29
Taylor M., Boch T., Fitzpatrick M., Allan A., Fay J., Paioro L., Taylor J., Tody D., 2012, IVOA Recommendation 2012-04-11: SAMP – Simple Application Messaging Protocol Version 1.3. International Virtual Observatory Alliance
Whitbourn J. R., Shanks T., 2014, MNRAS, 437, 2146
Wright E. L. et al., 2010, AJ, 140, 1868
Yasuda N. et al., 2001, AJ, 122, 1104

This paper has been typeset from a TEX/LATEX file prepared by the author.